EUROPEAN JOURNAL OF COMPUTATIONAL MECHANICS, 2015
VOL. 24, NO. 3, 107–128, http://dx.doi.org/10.1080/17797179.2015.1089462

Taylor & Francis
Taylor & Francis Group

A multilayered 3D hexahedral finite element with rotational DOFs

Kamel Meftah[a], Lakhdar Sedira[b], Wajdi Zouari[c], Rezak Ayad[c] and Mabrouk Hecini[b]

[a]Laboratoire de Génie Energétique et Matériaux, LGEM, University of Biskra, BP 145, RP, 07000 Biskra, Algeria; [b]Laboratoire de Génie Mécanique, LGM, University of Biskra, BP 145, RP, 07000 Biskra, Algeria; [c]LISM, EA 4695, University of Reims Champagne-Ardenne IUT de Troyes, 9 Rue de Québec, 10026 Troyes, France

ABSTRACT

The study presents a multilayer eight-node hexahedral finite element with rotational degree of freedom to model composite laminate structures. Its formulation is based on virtual rotations of a nodal fibre within the element that enriches the displacement vector approximation. A particular attention is made to the determination of transverse deflections as well as in-plane stresses. To assess the accuracy of the proposed element, several benchmarks are considered and the obtained results are compared with 3D elasticity solutions and other advanced finite elements from the literature.

ARTICLE HISTORY
Received 22 December 2015
Accepted 30 August 2015

KEYWORDS
3D finite element; multilayer solid element; rotational DOFs; composite structures

1. Introduction

Composite materials are used in many fields such as aerospace, mechanical and automotive industries, thanks to their high specific stiffness and strength, corrosive resistance and low coefficients of thermal expansion. In particular, composite laminated structures have extensively been used and are among many important structural applications made of composite materials. The behaviour of composite laminates can be characterised by complex 3D stress states, evidencing high interlaminar stresses caused by out-of-plane loading, curved geometry and the inherent anisotropy of material properties (Han & Hoa, 1993; Ramtekkar, Desai, & Shah, 2003). Among the different numerical techniques, the finite element method is an efficient technique and conventionally used to solve a wide range of practical problems involving laminated composite structures. Many composite multilayered plate and shell finite elements have been proposed for efficient analysis of laminated composite structures; see, e.g. References (Ayad, Talbi, & Ghomari, 2009;

CONTACT Kamel Meftah Meftah.kamel@gmail.com

Noor, Bert, & Burton, 1996; Noor, Burton, & Peters, 1991; Palazotto & Dennis, 1992; Reddy, 1989; Sedira, Ayad, Sabhi, Hecini, & Sakami, 2012). Reviews of some composite plate and shell elements can be found in Zhang and Yang (2009) and Yang, Saigal, Masud, and Kapania (2000), respectively. However, these elements are insufficient to analyse thick structures, since the zero transverse normal stress condition must be imposed (Simo, Rifai, & Fox, 1990). Therefore, the use of 3D solid elements, and especially the multilayer ones, gains an increasing interest in numerical modelling of composite structures because they help to accurately study regions subjected to 3D stress states and accordingly safely design these structures.

The development of 3D finite elements for the analysis of laminated composite structures has recently received a lot of attention by researchers because shell theories, which are based on simplified assumptions across the thickness, come to their limits of validity. 3D partial-hybrid and mixed multilayer solid elements dealing with a detailed stress analysis of multilayer composites, and in particular interlaminar transverse stresses, were introduced in Han and Hoa (1993), Harrison and Johnson (1996), and Feng, Hoa, and Huang (1997). The book of Van Hoa and Feng (1998) offers comprehensive overviews of the hybrid finite elements for stress analysis of composites, where different types of such elements and their improvements are given. Numerous modifications of the composite solid element approach can be seen in References Roy and Sihn (2001), Sihn and Roy (2001), Icardi and Atzori (2004), and Mijuca (2010). In Marimuthu, Sundaresan, and Rao (2001, 2003), it is shown that the 3D layered brick element with mixed finite element formulation could constitute the best option for finding the interlaminar stresses and to study the deformation behaviour of multilayer structures. The authors have already shown that this element works well for predicting the interlaminar stresses and deformations for in-plane loading. In Reference Marimuthu et al. (2003), a mixed finite element formulation with a 20-node layered hexahedron element is employed to predict the displacements and interlaminar stresses in laminates subjected to transverse loading. Abdullah, Ferrero, Barrau, and Mouillet (2007) used a new solid hexahedron element to examine delamination in composite laminates. The eight-node solid is derived from a 20-node hexahedron element and has 3 translational and 3 rotational degrees of freedom (DOFs).

In view of these issues, various 3D finite element models have been proposed and used to study the stress singularity at the free-edge. For example, Icardi and Bertetto (1995) used a 20-node quadratic hexahedral element and a 15-node quadratic singular wedge element to analyse the stress singularity at the free-edge interface and at corners of laminated plates. Chen, Shah, and Chan (1996) and Lessard, Schmidt, and Shokrieh (1996) also used 20-node hexahedral isoparametric element to, respectively, evaluate the interfacial stress distributions and analyse the free-edge effect in composite laminates. In a subsequent work, Hu, Soutis, and Edge (1997) studied the interlaminar stress distributions around a circular hole in symmetric composite laminates using 3D finite element analysis. On the other hand, a 18-node, 3D mixed finite element model based on the displacement theory

satisfying fundamental elasticity relations was presented in Ramtekkar, Desai, and Shah (2002), Ramtekkar et al. (2003), and Desai, Ramtekkar, and Shah (2003a, 2003b). In particular, it was shown that this model is able to provide reliable predictions of laminated composites stresses and displacements. Moreover, a 27-node 3D hexahedral hybrid-interface finite element model was developed by Bambole and Desai (2007) using the minimum potential energy principle to analyse thick laminated composite and sandwich plates. A 3D multilayer element based on hierarchical shape functions was developed in Kuhlmann and Rolfes (2004), especially to analyse thick composite structures. In this model, the in-plane stresses are computed from the displacement approximation and the out-of-plane stresses from the 3D equilibrium equations which require high-order interpolation functions.

The so-called space fibre rotation (SFR) concept was firstly introduced by Ayad (2002) to enhance the accuracy of first-order finite elements. It is based on the 3D virtual rotations of a nodal fibre that enriches the approximation of the displacement vector. This SFR concept was then adapted to 3D elastic structures in Meftah, Ayad, and Hecini (2013) by developing a 3D six-node wedge element, named SFR6, and in Ayad, Zouari, Meftah, Zineb, and Benjeddou (2013) by introducing two 3D eight-node hexahedral elements named SFR8 and SFR8I. These SFR concept-based solid elements present three rotational and three translational DOFs per node. Some of the solid elements with rotational DOFs can be found in Yunus, Pawlak, and Cook (1991) and Sze and Ghali (1993). In particular, it was shown in Meftah (2013), Meftah et al. (2013), and Ayad et al. (2013) that these 3D solid elements results are significantly better than the classical first-order wedge and hexahedral elements and globally close to those of the classical quadratic ones in the elastic isotropic case.

In this work, we propose a multilayered extension of the eight-node hexahedral element SFR8 (Ayad et al., 2013) to study composite laminate structures. Hence, the element has six DOFs per node, i.e. three displacements and three rotational parameters. Several plies in each hexahedral element are directly considered in the formulation to construct the stiffness matrix of the multilayer hexahedral element named SFR8M. Accordingly, only one element could be used across the thickness to model multilayer structures which results in a significant reduction of the computing cost as well as an acceptable model size when compared with models using at least one element per layer. The in-plane stress quantities (σ_x, σ_y and σ_{xy}) are determined from the enhanced displacement fields using the constitutive law, giving accurate predictions of these quantities.

This study is structured as follows. In Section 2, the formulation of the SFR concept-based eight-node hexahedral element SFR8 is reviewed and adapted to analyse laminated composite structures. Once the displacement vector approximation is defined and the stiffness matrix is obtained, in-plane stresses expressions are derived in Section 3. Finally, and before the concluding remarks, several numerical examples are presented in Section 4 to assess the accuracy of the proposed multilayered element.

2. The SFR concept finite element approximation

In order to derive the stiffness matrix of the eight-node multilayer hexahedral element SFR8M, the SFR concept is briefly recalled.

2.1. Kinematics of the SFR concept

The SFR concept, originally proposed by Ayad (2002), is based on the consideration of a nodal fibre within the element that enhances the mechanical displacement vector approximation after a virtual 3D rotation. Figure 1(a) shows the geometry of the eight-node hexahedron in which a virtual fibre iq is introduced at the nodal level. The fibre rotation, represented by the rotation vector θ_i, generates an additional displacement vector that enriches the classical displacement field approximation, used to formulate the standard first-order solid elements. For the eight-node hexahedral element SFR8, the final SFR concept-based displacement field approximation takes then the following form (Ayad, 2002; Ayad et al., 2013):

$$\underline{U}(\xi,\eta,\zeta) = \sum_{i=1}^{8} N_i(\xi,\eta,\zeta)\left(\underline{U}_i + \underline{\theta}_i \wedge \underline{iq}\right);\ \underline{U}_q \equiv \underline{U} \tag{1}$$

where $\{U_i\} = \{U_i\ V_i\ W_i\}^T$ is the nodal displacement vector, N_i are the classical trilinear Lagrange interpolation functions associated with the eight-node hexahedral element given by:

$$N_i(\xi,\eta,\zeta) = \frac{1}{8}(1+\xi_i\xi)(1+\eta_i\eta)(1+\zeta_i\zeta) \text{ with } -1 \le \xi,\eta,\zeta \le +1 \tag{2}$$

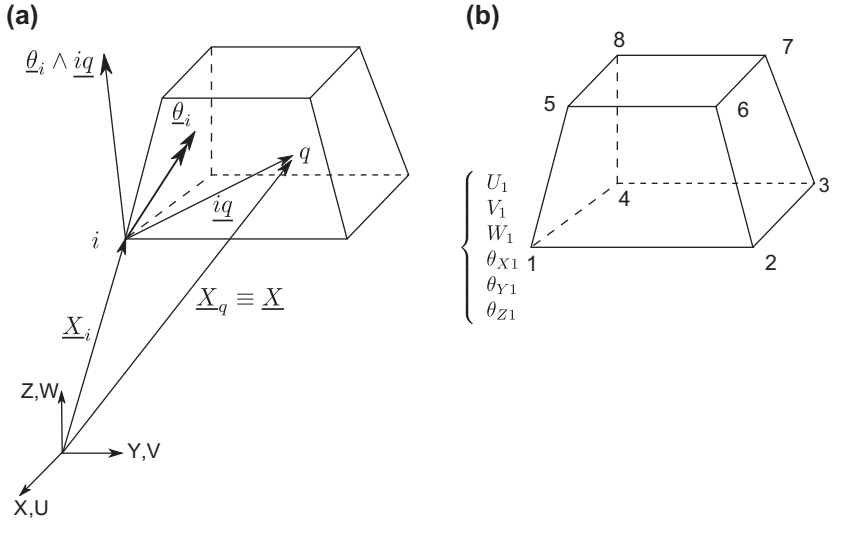

Figure 1. The SFR concept: (a) 3D rotation of the virtual fibre iq inducing an additional displacement, (b) the eight-node hexahedral element SFR8 and its nodal variables.

and

$$\{iq\} = \left\{X_q - X_i\right\} = \left\{\begin{array}{c} X - X_i \\ Y - Y_i \\ Z - Z_i \end{array}\right\}; \{\theta_i\} = \left\{\begin{array}{c} \theta_{X_i} \\ \theta_{Y_i} \\ \theta_{Z_i} \end{array}\right\} \tag{3}$$

X, Y and Z are the global coordinates of q given by the following approximations:

$$X = \sum_{i=1}^{8} N_i X_i; \quad Y = \sum_{i=1}^{8} N_i Y_i; Z = \sum_{i=1}^{8} N_i Z_i \tag{4}$$

where X_i, Y_i and Z_i are the global coordinates of node i. By performing the vector product $\underline{\theta}_i \wedge \underline{iq}$, we obtain the following approximation of the displacement vector $\underline{U}$:

$$\{U\} = \left\{\begin{array}{c} U \\ V \\ W \end{array}\right\} = \sum_{i=1}^{8} \left\{\begin{array}{c} N_i U_i + N_i(Z - Z_i)\theta_{Yi} - N_i(Y - Y_i)\theta_{Zi} \\ N_i V_i + N_i(X - X_i)\theta_{Zi} - N_i(Z - Z_i)\theta_{Xi} \\ N_i W_i + N_i(Y - Y_i)\theta_{Xi} - N_i(X - X_i)\theta_{Yi} \end{array}\right\} \tag{5}$$

The approximation (5) can be expressed in a matrix form:

$$\{U\} = [N]\left\{U_n\right\}; [N] = \left[\begin{array}{ccc} \cdots & \left\{N_{ui}\right\}^T & \\ & \left\{N_{vi}\right\}^T & \cdots \; i = 1,8 \\ & \left\{N_{wi}\right\}^T & \end{array}\right] = \left[\begin{array}{c} \left\{N_u\right\}^T \\ \left\{N_v\right\}^T \\ \left\{N_w\right\}^T \end{array}\right] \tag{6}$$

where

$$\left.\begin{array}{lcccccc} < N_{ui} > & = & N_i & 0 & 0 & 0 & +N_i(Z - Z_i) & -N_i(Y - Y_i) \\ < N_{vi} > & = & 0 & N_i & 0 & -N_i(Z - Z_i) & 0 & +N_i(X - X_i) \\ < N_{wi} > & = & 0 & 0 & N_i & +N_i(Y - Y_i) & -N_i(X - X_i) & 0 \end{array}\right\} \tag{7}$$

and

$$\left\{U_n\right\} = \left\{\begin{array}{ccccccccc} \cdots & U_i & V_i & W_i & \theta_{Xi} & \theta_{Yi} & \theta_{Zi} & \cdots & i = 1,8 \end{array}\right\}^T \tag{8}$$

is the nodal degree of freedom vector of SFR8 containing three translational and three rotational DOFs per node, see Figure 1(b).

2.2. The elastic strain tensor

In the global coordinate system, the strain tensor of q is classically defined by:

$$[\varepsilon] = \left[\begin{array}{ccc} \varepsilon_{XX} & \varepsilon_{XY} & \varepsilon_{XZ} \\ & \varepsilon_{YY} & \varepsilon_{YZ} \\ \text{Sym.} & & \varepsilon_{ZZ} \end{array}\right] \tag{9}$$

where

$$\varepsilon_{XX} = U_{,X};\ \varepsilon_{YY} = V_{,Y};\ \varepsilon_{ZZ} = W_{,Z};\ \gamma_{XY} = 2\varepsilon_{XY} = U_{,Y} + V_{,X} \quad \gamma_{XZ} = 2\varepsilon_{XZ} = U_{,Z} + W_{,X};\ \gamma_{YZ} = 2\varepsilon_{YZ} = V_{,Z} + W_{,Y} \tag{10}$$

Using expressions (10) of the mechanical strains and the approximation (6) of the displacement vector, we obtain a matrix relationship between the stain vector $\{\varepsilon\}$ and the nodal degree of freedom vector $\{U_n\}$:

$$\{\varepsilon\} = [B]\{U_n\};\ \underbrace{[B]}_{6\times 48} = \begin{bmatrix} \{N_{u,X}\}^T \\ \{N_{v,Y}\}^T \\ \{N_{w,Z}\}^T \\ \{N_{u,Y}\}^T + \{N_{v,X}\}^T \\ \{N_{u,Z}\}^T + \{N_{w,X}\}^T \\ \{N_{v,Z}\}^T + \{N_{w,Y}\}^T \end{bmatrix} \tag{11}$$

where

$$\begin{aligned} \langle N_{\alpha,x}\rangle &= j_{11}\langle N_{\alpha,\xi}\rangle + j_{12}\langle N_{\alpha,\eta}\rangle + j_{13}\langle N_{\alpha,\zeta}\rangle \\ \langle N_{\alpha,y}\rangle &= j_{21}\langle N_{\alpha,\xi}\rangle + j_{22}\langle N_{\alpha,\eta}\rangle + j_{23}\langle N_{\alpha,\zeta}\rangle;\ \alpha \equiv u, v, w \\ \langle N_{\alpha,z}\rangle &= j_{31}\langle N_{\alpha,\xi}\rangle + j_{32}\langle N_{\alpha,\eta}\rangle + j_{33}\langle N_{\alpha,\zeta}\rangle \end{aligned} \tag{12}$$

and j_{lk} are the inverse Jacobian matrix components ($[j] = [J]^{-1}$) with

$$[J] = \begin{bmatrix} X_{,\xi} & Y_{,\xi} & Z_{,\xi} \\ X_{,\eta} & Y_{,\eta} & Z_{,\eta} \\ X_{,\zeta} & Y_{,\zeta} & Z_{,\zeta} \end{bmatrix} \tag{13}$$

2.3. The element stiffness matrix

For linear elastic problems, the stiffness matrix of SFR8 takes the following simple form (Ayad et al., 2013):

$$[K^e] = \int_{V^e} [B]^T[C][B]\mathrm{d}V = \int_{-1}^{1}\int_{-1}^{1}\int_{-1}^{1} [B]^T[C][B]\det J\,\mathrm{d}\xi\mathrm{d}\eta\mathrm{d}\zeta \tag{14}$$

where $[C]$ is the elasticity matrix relating the stress and strain vectors.

The evaluation of $[K^e]$ is performed using the Gauss numerical integration technique. Typically, the elasticity matrix for a 3D multilayer structure is different from layer to layer, and thus it is not a continuous function of ζ. Therefore, the natural transverse coordinate of each layer $\zeta_k \in [-1, 1]$ is related to the third nat-

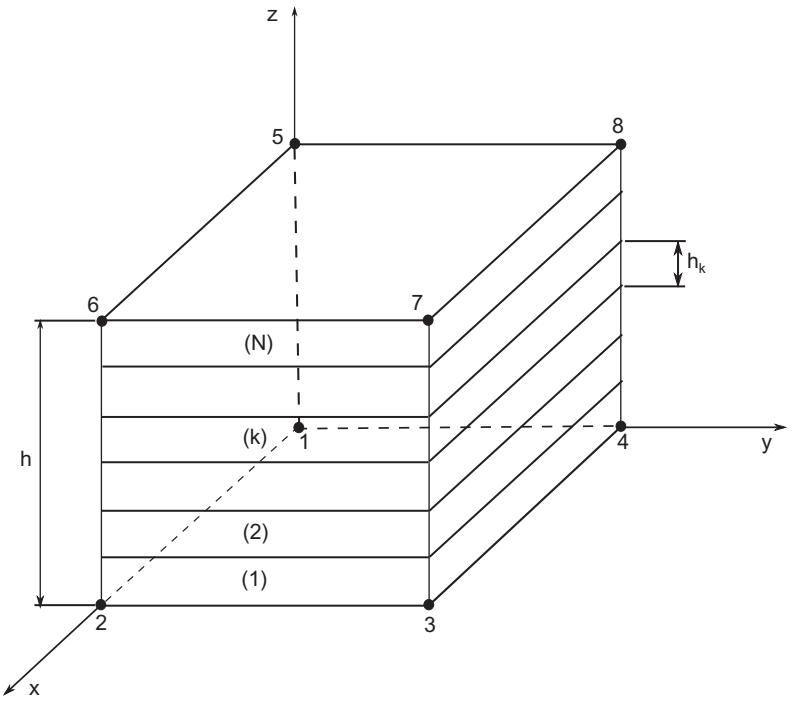

Figure 2. Geometry of the eight-node hexahedron multilayer element.

ural coordinate of the multilayer element $\zeta \in [-1, 1]$ by the following relationship (Kuhlmann & Rolfes, 2004; Mindlin, 1951):

$$\zeta = -1 + \frac{1}{h}\left(-h_k\left(1 - \zeta_k\right) + 2\sum_{j=1}^{k} h_j \right) \tag{15}$$

and

$$\frac{\partial \zeta}{\partial \zeta_k} = \frac{h_k}{h} \Rightarrow \partial \zeta = \frac{h_k}{h}\partial \zeta_k \tag{16}$$

By substituting (15) into (14), we obtain the final element stiffness matrix of the multilayer element SFR8M:

$$\left[K^e\right] = \sum_{k=1}^{N} \int_{-1}^{1}\int_{-1}^{1}\int_{-1}^{1} [B]^T \overset{(k)}{[C]} [B] \frac{h_k}{h} \det J \, \mathrm{d}\xi \mathrm{d}\eta \mathrm{d}\zeta_k \tag{17}$$

where N represents the total number of layers and h_k is the kth layer thickness, see Figure 2.

2.4. Constitutive equations

For a typical lamina (k) with principal axes (1-2-3), the stress–strain relation is given by:

$$\begin{Bmatrix} \sigma_{11} \\ \sigma_{22} \\ \sigma_{33} \\ \sigma_{12} \\ \sigma_{13} \\ \sigma_{23} \end{Bmatrix}^{(k)} = \begin{bmatrix} \bar{C}_{11} & \bar{C}_{12} & \bar{C}_{13} & 0 & 0 & 0 \\ & \bar{C}_{22} & \bar{C}_{23} & 0 & 0 & 0 \\ & & \bar{C}_{33} & 0 & 0 & 0 \\ & & & \bar{C}_{44} & 0 & 0 \\ & \text{Sym.} & & & \bar{C}_{55} & 0 \\ & & & & & \bar{C}_{66} \end{bmatrix}^{(k)} \cdot \begin{Bmatrix} \varepsilon_{11} \\ \varepsilon_{22} \\ \varepsilon_{33} \\ 2\varepsilon_{12} \\ 2\varepsilon_{13} \\ 2\varepsilon_{23} \end{Bmatrix}^{(k)} \tag{18}$$

where $\{\sigma_{11}\ \sigma_{22}\ \sigma_{33}\ \sigma_{12}\ \sigma_{13}\ \sigma_{23}\}^T$ and $\{\varepsilon_{11}\ \varepsilon_{22}\ \varepsilon_{33}\ 2\varepsilon_{12}\ 2\varepsilon_{13}\ 2\varepsilon_{23}\}^T$ are the stress and linear strain vectors referred to the lamina local coordinates system (1-2-3).

In terms of the engineering constants, $\bar{C}_{ij}$ are given by the following expressions:

$$\bar{C}_{11} = \frac{1 - \upsilon_{23}\upsilon_{32}}{\Delta} E_{11};\ \bar{C}_{22} = \frac{1 - \upsilon_{31}\upsilon_{13}}{\Delta} E_{22} \tag{19}$$

$$\bar{C}_{33} = \frac{1 - \upsilon_{21}\upsilon_{12}}{\Delta} E_{33};\ \bar{C}_{12} = \frac{\upsilon_{12} + \upsilon_{13}\upsilon_{32}}{\Delta} E_{22} \tag{20}$$

$$\bar{C}_{13} = \frac{\upsilon_{13} + \upsilon_{23}\upsilon_{12}}{\Delta} E_{33};\ \bar{C}_{23} = \frac{\upsilon_{23} - \upsilon_{21}\upsilon_{13}}{\Delta} E_{33} \tag{21}$$

$$\bar{C}_{44} = G_{12};\ \bar{C}_{55} = G_{13};\ \bar{C}_{66} = G_{23} \tag{22}$$

where

$$\Delta = 1 - \upsilon_{12}\upsilon_{21} - \upsilon_{23}\upsilon_{32} - \upsilon_{13}\upsilon_{31} - \upsilon_{12}\upsilon_{23}\upsilon_{31} - \upsilon_{21}\upsilon_{13}\upsilon_{32} \tag{23}$$

where E_i are Young's moduli, υ_{ij} are Poisson's ratios and G_{ij} are the shear moduli referred to the material coordinate system (1-2-3). For an arbitrary orientation of the layer, its local principal axes will not coincide with the global reference axes of the laminate; therefore, a rotational transformation should be performed. In a matrix form, this transformation is given by:

$$[C]^{(k)} = [T]\left[\bar{C}\right]^{(k)}[T]^T \tag{24}$$

where

$$[T] = \begin{bmatrix} c^2 & s^2 & 0 & -2cs & 0 & 0 \\ s^2 & c^2 & 0 & 2cs & 0 & 0 \\ 0 & 0 & 1 & 0 & 0 & 0 \\ cs & -cs & 0 & c^2 - s^2 & 0 & 0 \\ 0 & 0 & 0 & 0 & c & -s \\ 0 & 0 & 0 & 0 & s & c \end{bmatrix} \tag{25}$$

where $c = \cos(\theta)$, $s = \sin(\theta)$ in which θ is the angle between the global x-axis and the local 1-axis of each lamina. Using this transformation, the stress–strain relations in the global (x-y-z) coordinate system can be written as:

$$\begin{Bmatrix} \sigma_{xx} \\ \sigma_{yy} \\ \sigma_{zz} \\ \sigma_{xy} \\ \sigma_{xz} \\ \sigma_{yz} \end{Bmatrix} = \begin{bmatrix} C_{11} & C_{12} & C_{13} & C_{14} & 0 & 0 \\ & C_{22} & C_{23} & C_{24} & 0 & 0 \\ & & C_{33} & C_{34} & 0 & 0 \\ & & & C_{44} & 0 & 0 \\ & \text{Sym.} & & & C_{55} & C_{56} \\ & & & & & C_{66} \end{bmatrix} \cdot \begin{Bmatrix} \varepsilon_{xx} \\ \varepsilon_{yy} \\ \varepsilon_{zz} \\ 2\varepsilon_{xy} \\ 2\varepsilon_{xz} \\ 2\varepsilon_{yz} \end{Bmatrix} \tag{26}$$

where $\{\sigma_{xx}\,\sigma_{yy}\,\sigma_{zz}\,\sigma_{xy}\,\sigma_{xz}\,\sigma_{yz}\}^T$ and $\{\varepsilon_{xx}\,\varepsilon_{yy}\,\varepsilon_{zz}\,2\varepsilon_{xy}\,2\varepsilon_{xz}\,2\varepsilon_{yz}\}^T$ are the stress and linear strain vectors with respect to the laminate axes (x-y-z).

2.5. Numerical integration

In the definition of the displacement field vector in Equation (5), the approximation of the part corresponding to the virtual nodal rotations is quadratic in terms of ξ, η and ζ. Consequently, a $3 \times 3 \times 3$ Gauss point's scheme is necessary to exactly determine the stiffness matrix. In order to render the multilayer element SFR8M computationally more effective, the reduced integration scheme with $2 \times 2 \times 2$ Gauss points for each layer is adopted. Accordingly, the stiffness matrix coefficients are calculated as:

$$\left[K^e\right] = \sum_{k=1}^{N} \sum_{l=1}^{2} \sum_{m=1}^{2} \sum_{i=1}^{2} \left([B]^T [C]^{(k)} [B] \frac{h_k}{h} DetJ \; w_1^i w_2^m w_3^l \right)_{(\xi_i^k, \eta_m^k, \zeta_l^k)} \tag{27}$$

where ξ_i^k, η_m^k and ζ_l^k are the Gauss points coordinates of the kth layer and w_1^i, w_2^m and w_3^l represent their corresponding Gaussian weights. Consequently, the total number of Gauss points per element is equal to $(2 \times 2 \times 2) \times N$.

3. In-plane stresses

The stress vector of the kth is classically determined using the constitutive law and takes the following form:

$$\{\sigma\}^{(k)} = \{C\}^{(k)} \{\varepsilon\} = \{C\}^{(k)} [B] \left\{U_n\right\} \tag{28}$$

As considered in References Van Hoa and Feng (1998) and Kuhlmann and Rolfes (2004), the stress and strain vectors can be divided into two in-plane and transverse parts:

$$\{\sigma_L\}^{(k)} = \begin{Bmatrix} \sigma_x \\ \sigma_y \\ \tau_{xy} \end{Bmatrix}^{(k)}; \{\sigma_G\}^{(k)} = \begin{Bmatrix} \sigma_z \\ \tau_{xz} \\ \tau_{yz} \end{Bmatrix}^{(k)} \tag{29}$$

$$\{\varepsilon_G\} = \begin{Bmatrix} \varepsilon_x \\ \varepsilon_y \\ \gamma_{xy} \end{Bmatrix}; \{\varepsilon_L\} = \begin{Bmatrix} \varepsilon_z \\ \gamma_{xz} \\ \gamma_{yz} \end{Bmatrix} \tag{30}$$

where (G) and (L) denote, respectively, the global and local variables. In contrast to the global variables, which are continuous across the thickness of the laminate and therefore at the layer interfaces, local ones are continuous only across the thickness of each layer but not at the layer interfaces (Kuhlmann & Rolfes, 2004).

The stress–strain relationship can then be expressed as:

$$\begin{Bmatrix} \{\sigma_L\} \\ \{\sigma_G\} \end{Bmatrix}^{(k)} = \begin{bmatrix} [C_1] & [C_2] \\ [C_2] & [C_3] \end{bmatrix}^{(k)} \begin{Bmatrix} \{\varepsilon_G\} \\ \{\varepsilon_L\} \end{Bmatrix} \tag{31}$$

and hence, the in-plane stresses are given by:

$$\{\sigma_L\}^{(k)} = \begin{bmatrix} [C_1] & [C_2] \end{bmatrix}^{(k)} \begin{Bmatrix} \{\varepsilon_G\} \\ \{\varepsilon_L\} \end{Bmatrix} = [C_L]^{(k)}[B]\,[U_n] \tag{32}$$

4. Numerical results and discussion

The performances of the new multilayer solid element SFR8M for static analysis of laminated composite structures are demonstrated through four numerical examples. The accuracy of the present element as well as the in-plane stress predictions are studied and principally compared with 3D elasticity exact solutions and other advanced finite element models. The first two numerical examples focus on simply supported rectangular layered composite plates (Figure 3) under the sinusoidal load: $\bar{q}(x,y) = q_0 \sin(\pi x/a)\sin(\pi y/b)$; $q_0 = 1$ MPa. The length, width and thickness of the plate is denoted by a, b and h, respectively. The laminate is made of material plies that are idealised to be homogeneous, elastic and orthotropic. The obtained transverse displacement and in-plane stresses results are rendered dimensionless as follows:

$$\bar{\sigma}_x = \frac{1}{q_0.S^2}\sigma_x(0,0,z);\ \bar{\sigma}_y = \frac{1}{q_0.S^2}\sigma_y(0,0,z);\ \bar{\sigma}_{xy} = \frac{1}{q_0.S^2}\sigma_{xy}\left(\frac{a}{2},\frac{b}{2},z\right) \tag{33}$$

$$\bar{w} = \frac{100E_2}{h.q_0.S^4}w(0,0,z);\ S = \frac{a}{h};\ \bar{z} = \frac{z}{h} \tag{34}$$

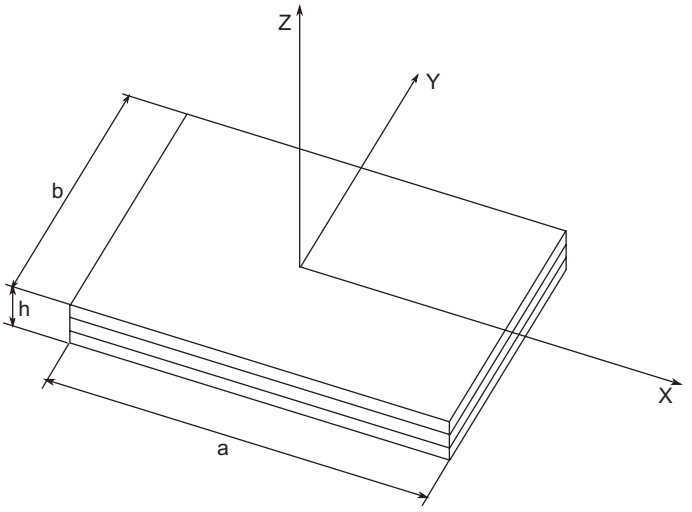

Figure 3. Simply supported rectangular laminated plate.

On the other hand, the effect of mesh distortion on finite element accuracy is investigated in the third example by considering a cantilever beam meshed with six elements. In the fourth example, a single-layer hollow composite cylinder under internal pressure was employed to evaluate the performance of the proposed element in shell composite structures.

4.1. A simply supported four-layered (0°/90°/90°/0°) square plate under sinusoidal transverse load

We consider in this first example a simply supported four-layered (0°/90°/90°/0°) laminate plate under sinusoidal load. The plate has the same lamination geometry and $L = b = a$. The material properties of this multilayer plate are

$$E_1 = 250 \text{ GPa}; E_2 = E_3 = 10 \text{ GPa}; \nu_{12} = \nu_{23} = \nu_{13} = .25$$
$$G_{12} = G_{13} = 5 \text{ GPa}; G_{23} = 2 \text{ GPa}$$

A mesh of 5 × 5 elements in the *x*-*y* plane and two elements along the thickness direction are used to model the multilayer plate. The dimensionless central transverse deflection variation with respect to the plate slenderness ratio ($S = L/h$) is shown in Figure 4. A good agreement is found between the SFR8M result and the 3D elasticity solution reported in Pagano (1970) and the results obtained by Pandya and Kant (1988) by considering the higher order plate theory.

The variation of the dimensionless in-plane stress ($\bar{\sigma}_x$) with respect to the plate length-to-thickness ratio ($S = L/h$) is depicted in Figure 5 where a comparison between SFR8M, the 3D multilayer element proposed by Kuhlmann and Rolfes (2004) (with 5 × 5 × 2 mesh) and the 3D elasticity solution (Pagano, 1970) is

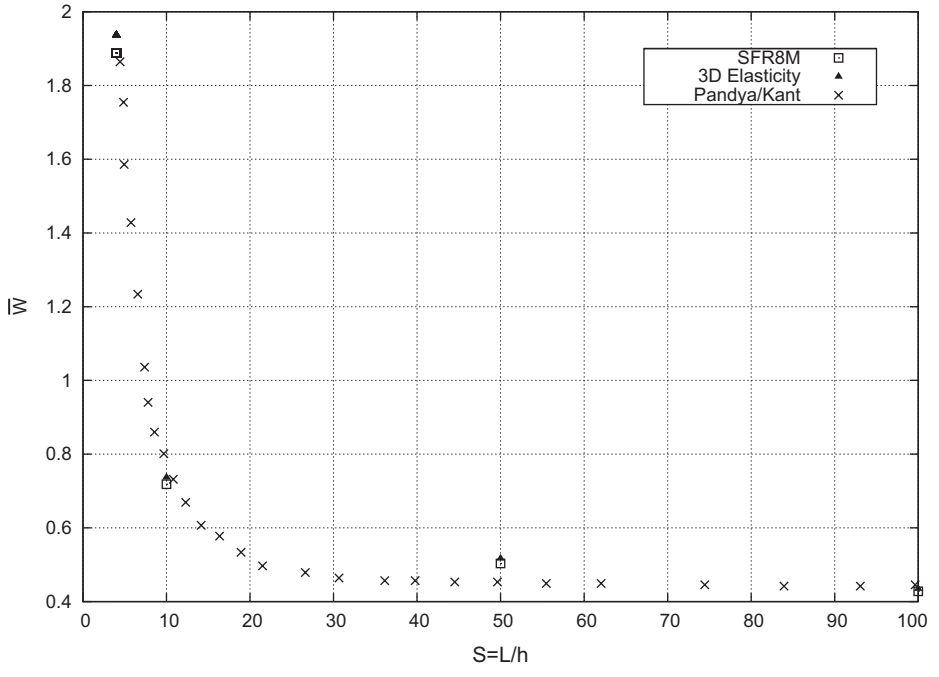

Figure 4. Effect of the plate slenderness ratio on the dimensionless central deflection ($\bar{w}$) of the simply supported (0°/90°/90°/0°) cross-ply square laminate under sinusoidal transverse load.

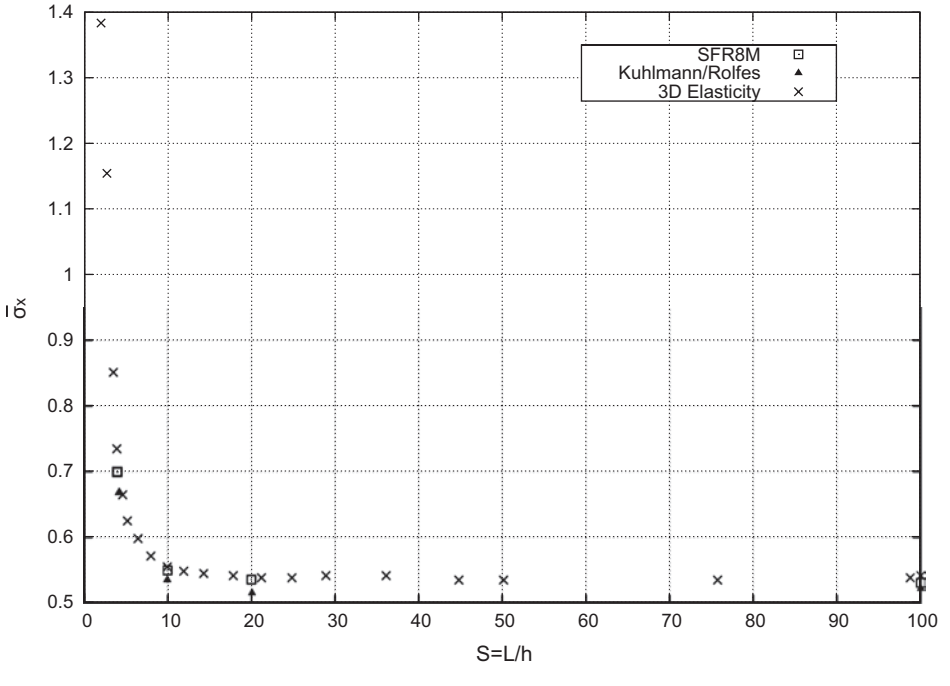

Figure 5. Effect of the plate slenderness ratio (L/h) on the dimensionless in-plane stress ($\bar{\sigma}_x$) of the simply supported (0°/90°/90°/0°) cross-ply square laminate under sinusoidal transverse load.

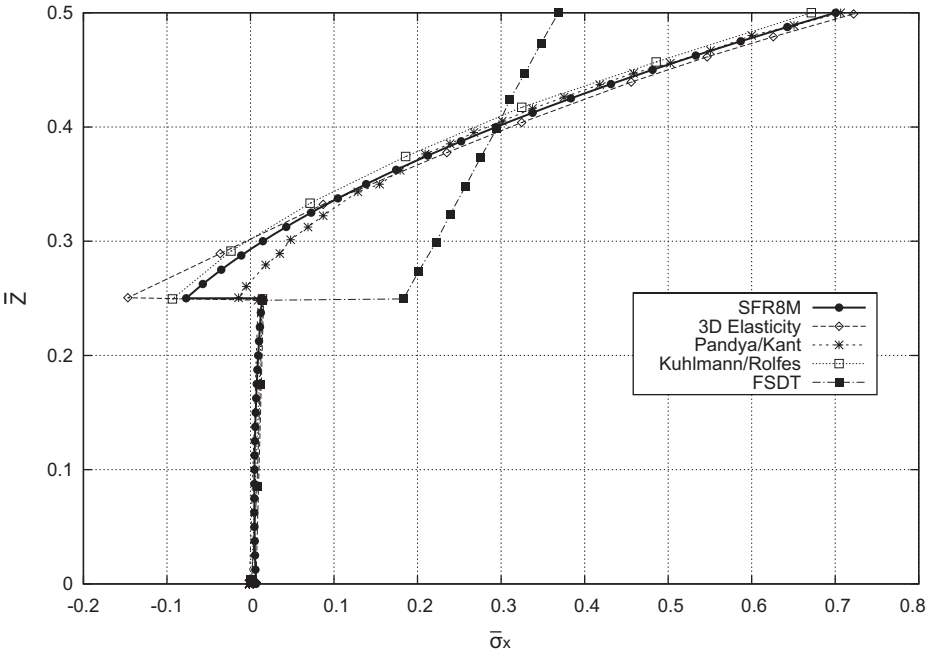

Figure 6. The dimensionless in-plane stress ($\bar{\sigma}_x$) distribution across the thickness of the simply supported (0°/90°/90°/0°) cross-ply square laminate subjected to a sinusoidal transverse load ($L/h = 4$).

Table 1. Results of the dimensionless centroidal deflection and the in-plane stresses of a simply supported (0°/90°/90°/0°) cross-ply square laminate under sinusoidal transverse load (the quantity inside parentheses indicates the normalised displacement and in-plane stresses).

L/h	Model (mesh)	$\bar{w}(0)$	$\bar{\sigma}_{xx}(h/2)$	$\bar{\sigma}_{yy}(h/4)$	$\bar{\sigma}_{xy}(h/2)$
10	3D elasticity	.7370	.5590	.4010	.0275
	HSDT	.7147 (.969)	.5456 (.981)	.3888 (.969)	.0268 (.974)
	SFR8M (5 × 5 × 2)	.7188 (.975)	.5526 (.988)	.3874 (.966)	.0268 (.974)
	SFR8M (8 × 8 × 2)	.7254 (.984)	.5567 (.995)	.3988 (.994)	.0272 (.989)
	SFR8M (16 × 16 × 2)	.7367 (.999)	.5590 (1.000)	.4009 (.999)	.0274 (.996)
100	3D elasticity	.4347	.5390	.2710	.0214
	HSDT	.4343 (.999)	.5387 (.999)	.2708 (.999)	.0213 (.995)
	SFR8M (5 × 5 × 2)	.4290 (.986)	.5324 (.987)	.2660 (.981)	.0211 (.985)
	SFR8M (8 × 8 × 2)	.4311 (.991)	.5352 (.992)	.2696 (.994)	.0212 (.990)
	SFR8M (16 × 16 × 2)	.4344 (.999)	.5389 (.999)	.2708 (.999)	.0214 (1.000)

presented. Once again, we remark that the SFR8M in-plane stress ($\bar{\sigma}_x$) results are in excellent agreement with the 3D elasticity solutions.

The through-the-thickness variation of the dimensionless in-plane stress ($\bar{\sigma}_x$) is presented in Figure 6 for the aspect ratio $S = L/h = 4$. In this figure, the results obtained by SFR8M are compared with the 3D elasticity solution (Pagano, 1970), the higher order plate theory (Pandya & Kant, 1988), the 3D multilayer element proposed in Kuhlmann and Rolfes (2004) and the first-order shear deformation theory (FSDT) presented by Whitney and Pagano (1970). It should be noticed

that the results provided by the FSDT are not in a good agreement with those of the 3D elasticity for moderately thick plates. As already explained in Kuhlmann and Rolfes (2004), the higher order plate theory does not predict accurately the stress value at the internal interface. The results obtained by SFR8M agree well with the 3D elasticity solution and are close to those of the 3D multilayer finite element developed in Kuhlmann and Rolfes (2004).

Table 1 summarises the results of the dimensionless central deflection and in-plane stresses for two slenderness ratios L/h = 10 and 100. In addition to the 3D elasticity results, we show also those of the higher deformation plate theory developed in Reddy (1984). Specifically, results by the regular meshes 5 × 5 × 2, 8 × 8 × 2 and 16 × 16 × 2 are presented to investigate the effect of mesh refinement. The convergence of normalised displacement and in-plane stresses is given in parentheses in Table 1. The SFR8M response is found to be close and converges to the 3D elasticity solution and remains stable when we increase the slenderness of the plate.

4.2. A simply supported three-layered (0°/90°/0°) square plate under sinusoidal transverse load

The second example considers a three-layered (0°/90°/0°) simply supported square laminated plate under sinusoidal load: $\bar{q}(x,y) = q_0 \sin(\pi x/a)\sin(\pi y/b)$; $q_0 = 1$ MPa. A regular mesh constituted of 8 × 8 elements on the x-y plane and two across the thickness is used to model the multilayer plate. The material properties of this second plate are similar to those used in the first example. Figure 7 shows the distributions of the dimensionless central deflection through the laminate thickness, for the aspect ratios $S = L/h$ = 2, 4, 10 and 100, predicted by SFR8M and compared with the 3D elasticity solution (Pagano, 1970). We remark that, except for the first slenderness ratio L/h = 2, the SFR8M responses agree very well with the 3D analytical solution. The through-the-thickness distributions of the dimensionless in-plane stresses $\bar{\sigma}_x$ and $\bar{\sigma}_{xy}$ for the slenderness ratio $S = L/h$ = 4 are depicted in Figures 8 and 9, respectively. The SFR8M predictions agree globally well with the 3D elasticity solution. However, a remarkable difference is found at the 0°/90° interfaces for the $\bar{\sigma}_x$ distribution.

Typical convergence trend for simply supported cross-ply laminated (0°/90°/0°) square plate with slenderness ratio $S = L/h$ = 4, 10 and 100 is presented in Table 2. The numbers in parentheses of Table 2 show the convergence rate of normalised displacement and in-plane stresses. We remark that SFR8M present good responses and converge quickly to the reference solution.

4.3. The effect of mesh distortion

A cantilever beam subjected to unit in-plane and out-of-plane loads at the free end is examined in this section as shown in Figure 10. This example, studied by Bussamra,

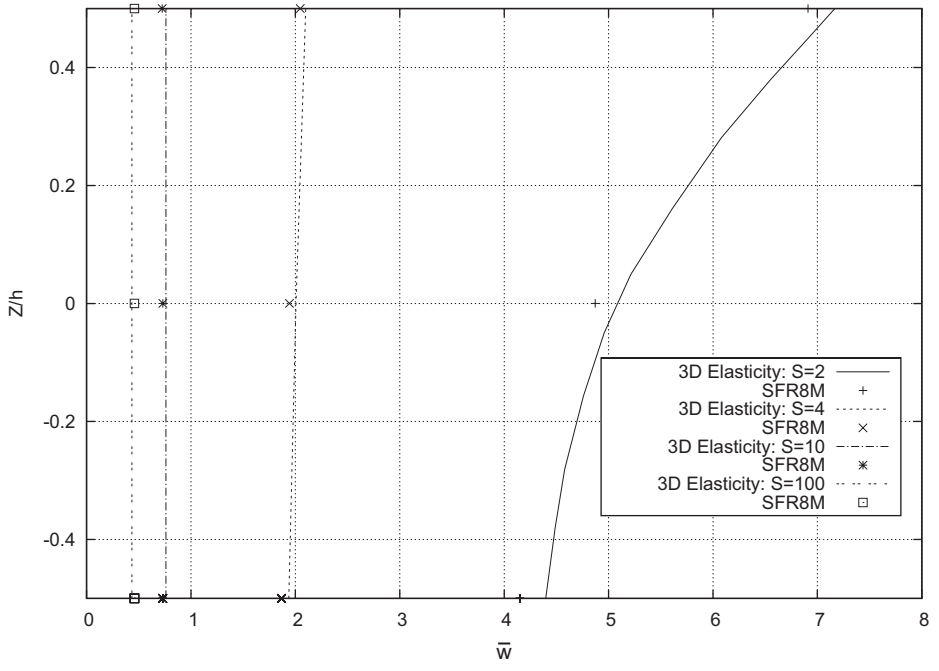

Figure 7. The dimensionless transverse displacement $\bar{w}(0,0)$ distribution across the thickness of the (0°/90°/0°) laminate for $L/h = 2$, 4, 10 and 100.

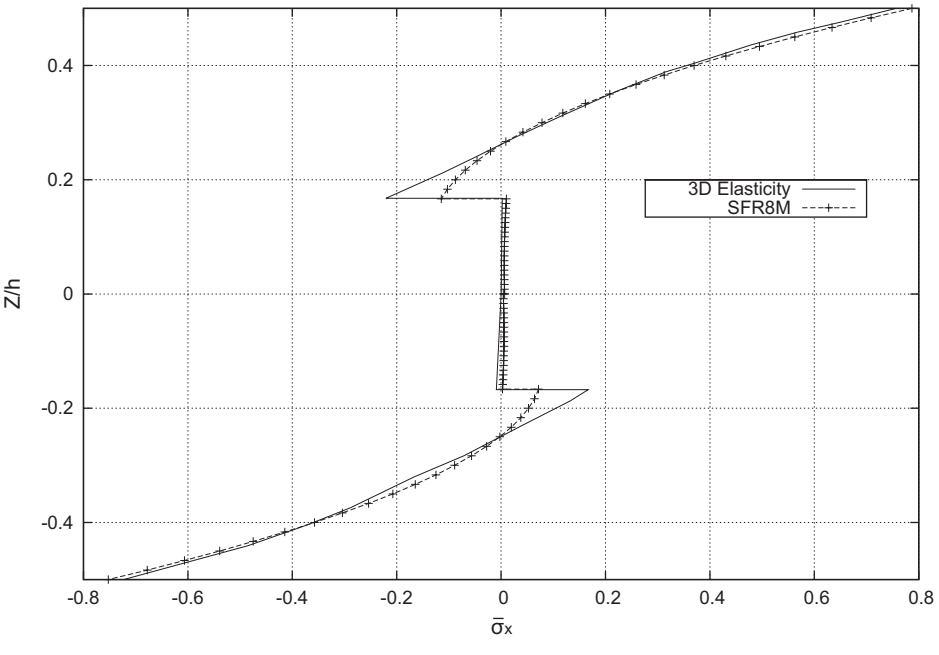

Figure 8. The dimensionless in-plane stress $\bar{\sigma}_x$ distribution across the thickness for the simply supported (0°/90°/0°) cross-ply square laminate under sinusoidal transverse load with ($L/h = 4$).

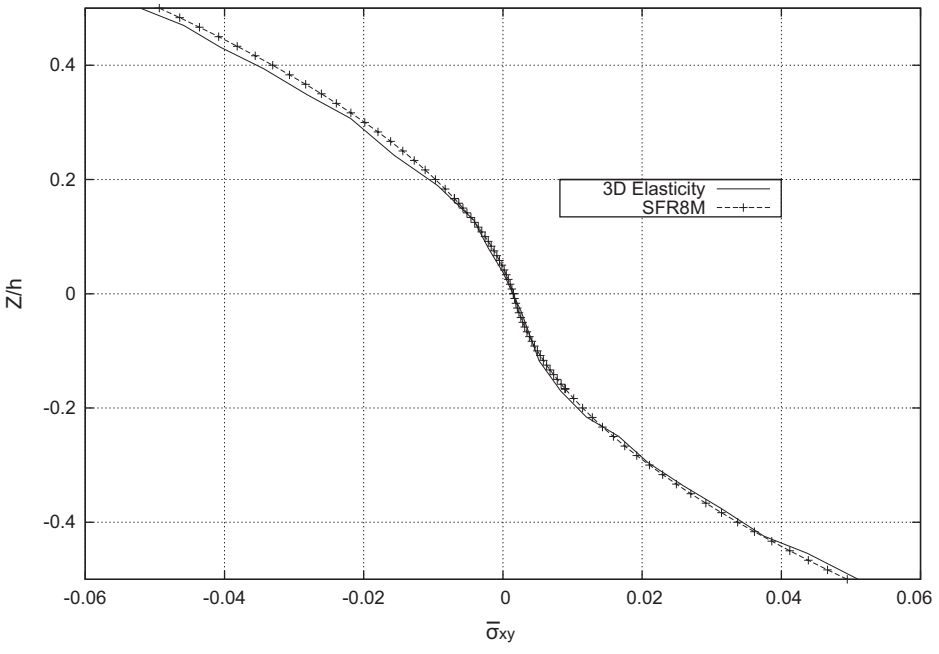

Figure 9. The dimensionless in-plane stress $\bar{\sigma}_{xy}$ distribution across the thickness for the simply supported (0°/90°/0°) cross-ply square laminate under sinusoidal transverse load ($L/h = 4$).

Table 2. Convergence results of the dimensionless vertical displacement and in-plane stresses of a simply supported (0°/90°/0°) cross-ply square laminate under sinusoidal transverse load (the quantity inside parentheses indicates the normalised displacement and in-plane stresses).

L/h	Model (mesh)	$\bar{w}(0)$	$\bar{\sigma}_{xx}(h/2)$	$\bar{\sigma}_{yy}(h/6)$	$\bar{\sigma}_{xy}(h/2)$
4	3D elasticity	2.01	.755	.556	−.0511
	SFR8M (2 × 2 × 2)	1.78 (.887)	.672 (.891)	.493 (.888)	−.0454 (.890)
	SFR8M (4 × 4 × 2)	1.89 (.941)	.722 (.957)	.531 (.956)	−.0486 (.952)
	SFR8M (8 × 8 × 2)	1.94 (.969)	.785 (1.04)	.554 (.998)	−.0494 (.967)
	SFR8M (16 × 16 × 2)	2.00 (.999)	.770 (1.02)	.555 (.999)	−.0511 (1.000)
10	3D elasticity	.753	.590	.285	−.0289
	SFR8M (2 × 2 × 2)	.664 (.883)	.523 (.887)	.253 (.888)	−.0256 (.886)
	SFR8M (4 × 4 × 2)	.716 (.952)	.566 (.960)	.273 (.959)	−.0276 (.956)
	SFR8M (8 × 8 × 2)	.731 (.971)	.577 (.979)	.279 (.981)	−.0282 (.978)
	SFR8M (16 × 16 × 2)	.751 (.998)	.588 (.998)	.285 (1.000)	−.0288 (.998)
100	3D elasticity	.435	.539	.181	−.0213
	SFR8M (2 × 2 × 2)	.392 (.902)	.485 (.901)	.163 (.904)	−.0194 (.911)
	SFR8M (4 × 4 × 2)	.417 (.960)	.515 (.957)	.173 (.958)	−.0203 (.955)
	SFR8M (8 × 8 × 2)	.452 (1.04)	.534 (.991)	.179 (.992)	−.0211 (.995)
	SFR8M (16 × 16 × 2)	.443 (1.02)	.538 (.999)	.181 (1.000)	−.0213 (1.000)

Neto, and Raimundo (2012), is a famous benchmark for testing the sensitivity of finite elements to mesh distortion and it is considered here to verify the SFR8M formulation without layered configurations. As depicted in Figure 10, the cantilever beam is modelled with one six-elements regular mesh (mesh A) and two distorted meshes (meshes B and C). Two isotropic and orthotropic materials are used in this benchmark as in Bussamra et al. (2012) and their properties are given by:

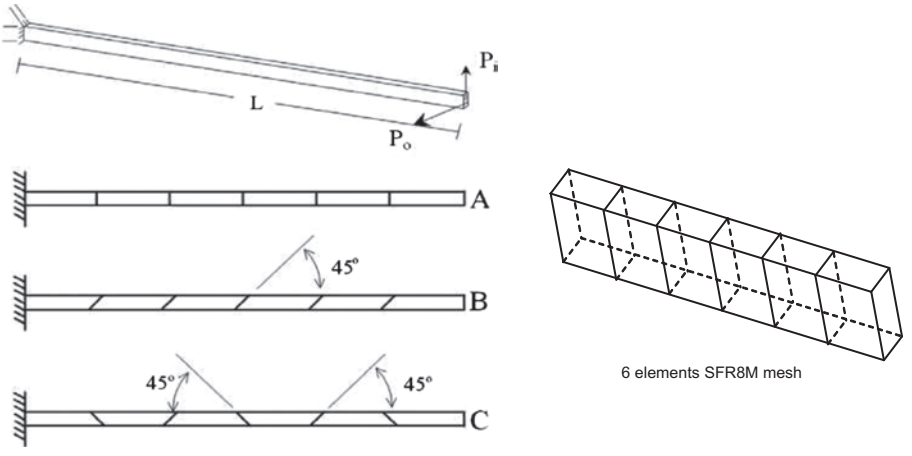

Figure 10. Cantilever beam for mesh distortion test.

Table 3. Normalised tip displacements for the cantilever beam.

Material	Isotropic						Orthotropic					
Load	In-plane			Out-of-plane			In-plane			Out-of-plane		
Mesh	A	B	C	A	B	C	A	B	C	A	B	C
HEXA8(SR)	.981	.080	.069	.961	.055	.051	.992	.182	.138	.993	.069	.069
HEXA16	.975	.817	.898	.970	.820	.961	.996	.908	.968	.998	.930	.990
HEX20	.970	.967	.886	.961	.941	.920	–	–	–	–	–	–
HEX8X	.978	.624	.047	.973	.528	.030	–	–	–	–	–	–
SFR8M	.886	.845	.797	.895	.885	.869	.969	.907	.860	.972	.971	.956

$E = 10^7$, $\nu = .3$ the isotropic material
$E_1 = 4E_2 = 5E_3 = 10^7$; $G_{12} = G_{13} = 5G_{23} = 3.846 \times 10^6$
$\nu_{12} = \nu_{13} = .3$; $\nu_{23} = .05$ the orthotropic material

Table 3 presents the normalised results of SFR8M element compared with those of two NASTRAN hexahedral elements reported in Bussamra et al. (2012): the linear hexahedral element HEXA8(SR) with selective reduction integration and the parabolic element HEXA16. Moreover, the present element is also compared, for isotropic material, to the hexahedral finite element HEX8X with rotational DOFs developed by Yunus et al. (1991) and standard isoparametric 20-node second-order hexahedral element HEX20 reported in Macneal and Harder (1985). The reference displacements of the cantilever beam free end, for both the isotropic and orthotropic materials, are .1081 and .4321, for the in-plane and out-of-plane loads, respectively (Bussamra et al., 2012). We depict in Figure 11 the convergence curves of the present element in terms of the total degree of freedom number. We remark that SFR8M presents good results and converges more quickly to the reference solution. For the distorted meshes, SFR8M is found to more accurate than HEXA8(SR) and presents approximately the same results as the parabolic element HEXA16.

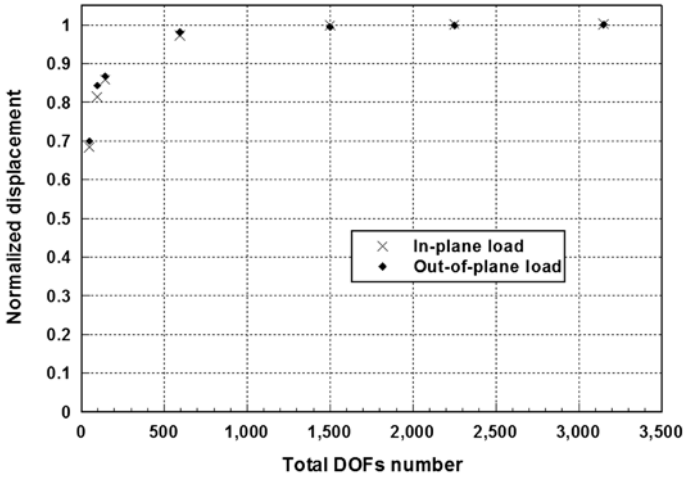

Figure 11. Convergence of normalised tip displacements for the cantilever beam.

4.4. Orthotropic cylindrical shell

Figure 12 shows a one-layered cylindrical composite shell, fully clamped ends, under uniform internal pressure (P). The geometric and material properties of this structure are shown in Table 4. Thanks to the symmetry of the structure, only one-eighth of the cylindrical shell is modelled with regular meshes $8 \times 8 \times 1$ (eight elements along the circumference and the length and one element across the thickness), $16 \times 16 \times 2$ and $32 \times 32 \times 2$. The vertical deflection at the centre of the shell obtained by SFR8M and the exact solution obtained by the thin shell theory given in Kraus (1967) are summarised in Table 5. In addition to that we also show the results obtained by hybrid-mixed shell element MiSP4-Q4 with 10×5 mesh presented in Ayad (2002). The results reported in Table 5 show an acceptable agreement between

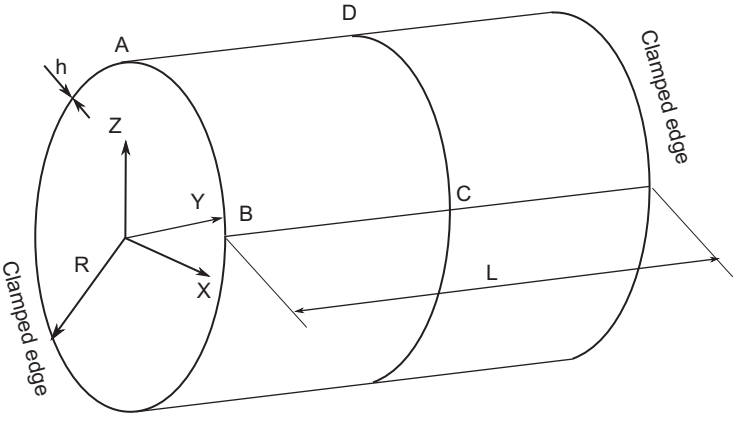

Figure 12. A single-layer orthotropic cylindrical shell.

Table 4. Geometric and material properties of the composite cylindrical shell.

$L = .5080$ m, $R = .5080$ m	$E_{11} = 1.379$ GPa, $E_{22} = E_{33} = 5.1711$ GPa
$h = .0254$ m, $p = 1$ Pa	$G_{12} = 8.6184$ GPa, $G_{13} = G_{23} = 4.3092$ GPa
	$\nu_{12} = \nu_{13} = \nu_{23} = .0667$

Table 5. Vertical deflections at the centre of the one-layered cylindrical composite shell (the quantity inside parentheses indicates the normalised displacement).

Mesh	SFR8M	MiSP4-Q4	Thin shell theory
$8 \times 8 \times 1$	$.720 \times 10^{-9}$ m (1.085)		
$16 \times 16 \times 2$	$.691 \times 10^{-9}$ m (1.042)		
$32 \times 32 \times 2$	$.688 \times 10^{-9}$ m (1.037)	$.684 \times 10^{-9}$ m (1.032)	$.663 \times 10^{-9}$ m

the SFR8M response and the thin shell theory. Moreover, SFR8M presents approximately the same results as the MiSP4-Q4 element reported in Ayad (2002).

5. Concluding remarks

A new multilayered solid element named SFR8M and based on the SFR concept was developed for the analysis of laminated composites. The displacement approximation of the classical eight-node hexahedral finite element is enriched by additional terms related to the virtual 3D rotations of a nodal fibre within the element. To assess the accuracy of the proposed multilayered element, some benchmarks were considered and the obtained results were compared especially with 3D elasticity solutions. In particular, it was shown that transverse deflections and in-plane stresses predicted by SFR8M agree well with the reference solutions. As a future work, the SFR8M formulation should be extended to the determination of transverse stresses, which constitute the main cause of delamination.

Disclosure statement

No potential conflict of interest was reported by the authors.

ORCID

Kamel Meftah http://orcid.org/0000-0002-5671-602X
Lakhdar Sedira http://orcid.org/0000-0003-1735-2195

References

Abdullah, E., Ferrero, J. F., Barrau, J. J., & Mouillet, J. B. (2007). Development of a new finite element for composite delamination analysis. *Composites Science and Technology, 67*, 2208–2218.

Ayad, R. (2002). *Contribution à la modélisation numérique pour l'analyse des solides et des structures, et pour la mise en forme des fluides non newtoniens. Application à des matériaux*

d'emballage [Contribution to the numerical modeling of solids and structures and the non-Newtonian fluids forming process. Application to packaging materials]. Habilitation to conduct researches, University of Reims, Reims, France. (in French).

Ayad, R., Talbi, N., & Ghomari, T. (2009). Modified discrete Mindlin hypothesises for laminated composite structures. *Composites Science and Technology, 69*, 125–128.

Ayad, R., Zouari, W., Meftah, K., Zineb, T. B., & Benjeddou, A. (2013). Enrichment of linear hexahedral finite elements using rotations of a virtual space fiber. *International Journal for Numerical Methods in Engineering, 95*, 46–70.

Bambole, A., & Desai, Y. (2007). Hybrid-interface element for thick laminated composite plates. *Computers and Structures, 85*, 1484–1499.

Bussamra, F., Neto, E. L., & Raimundo, D. R. Jr. (2012). Hybrid quasi-Trefftz 3-D finite elements for laminated composite plates. *Computers Structures, 92–93*, 185–192.

Chen, D., Shah, D., & Chan, W. (1996). Interfacial stress estimation using least-square extrapolation and local stress smoothing in laminated composites. *Computers and Structures, 58*, 765–774.

Desai, Y. M., Ramtekkar, G. S., & Shah, A. H. (2003a). Dynamic analysis of laminated composite plates using a layer-wise mixed finite element model. *Composite and Structures, 59*, 237–249.

Desai, Y. M., Ramtekkar, G. S., & Shah, A. H. (2003b). A novel 3D mixed finite-element model for statics of angle-ply laminates. *International Journal for Numerical Methods in Engineering, 57*, 1695–1716.

Feng, W., Hoa, S. V., & Huang, Q. (1997). Classification of stress modes in assumed stress fields of hybrid finite elements. *International Journal for Numerical Methods in Engineering, 40*, 4313–4339.

Han, J., & Hoa, S. V. (1993). A three-dimensional multilayer composite finite element for stress analysis of composite laminates. *International Journal for Numerical Methods in Engineering, 36*, 3903–3914.

Harrison, P. N., & Johnson, E. R. (1996). A mixed variational formulation for interlaminar stresses in thickness-tapered composite laminates. *International Journal of Solids and Structures, 33*, 2377–2399.

Hu, F., Soutis, C., & Edge, E. (1997). Interlaminar stresses in composite laminates with a circular hole. *Composite and Structures, 37*, 223–232.

Icardi, U., & Atzori, A. (2004). Simple, efficient mixed solid element for accurate analysis of local effects in laminated and sandwich composites. *Advances in Engineering Software, 35*, 843–859.

Icardi, U., & Bertetto, A. (1995). An evaluation of the influence of geometry and of material properties at free edges and at corners of composite laminates. *Computers and Structures, 57*, 555–571.

Kraus, H. (1967). *Thin elastic shells: An introduction to the theoretical foundations and the analysis of their static and dynamic behavior*. New York, NY: John Wiley & Sons, University of California.

Kuhlmann, G., & Rolfes, R. (2004). A hierarchic 3D finite element for laminated composites. *International Journal for Numerical Methods in Engineering, 61*, 96–116.

Lessard, L. B., Schmidt, A. S., & Shokrieh, M. M. (1996). Three-dimensional stress analysis of free-edge effects in a simple composite cross-ply laminate. *International Journal of Solids and Structures, 33*, 2243–2259.

Macneal, R. H., & Harder, R. L. (1985). A proposed standard set of problems to test finite element accuracy. *Finite Elements in Analysis and Design, 1*, 3–20.

Marimuthu, R., Sundaresan, M., & Rao, G. (2001). Estimation of interlaminar normal and shear stresses by three-dimensional hexahedron element using mixed finite element formulation. *Journal of the Institution of Engineers, 82*, 50–55.

Marimuthu, R., Sundaresan, M., & Rao, G. (2003). Estimation of interlaminar stresses in laminated plates subjected to transverse loading using three-dimensional mixed finite element formulation the institution of engineers (India). *Technical Journal of Aerospace Engineering, 84*, 1–8.

Meftah, K. (2013). *Modélisation numérique des solides par éléments finis volumiques basés sur le concept SFR* [Numerical modeling of 3D structure by solid finite elements based upon the SFR concept]. (Space Fiber Rotation) (PhD thesis). University of Biskra, Algeria. (in French).

Meftah, K., Ayad, R., & Hecini, M. (2013). A new 3D 6-node solid finite element based upon the space fibre rotation concept. *European Journal of Computational Mechanics, 22*(1), 1–29.

Mijuca, D. (2010). On a new 3D primal-mixed finite element approach for thermal stress analysis of multi-layered geometrically multiscale structures. *Finite Elements in Analysis and Design, 46*, 299–310.

Mindlin, R. D. (1951). Influence of rotary inertia and shear on flexural motions of isotropic, elastic plates. *Journal of Applied Mechanics, 18*, 31–38.

Noor, A. K., Bert, C. W., & Burton, W. S. (1996). Computational models for sandwich panels and shells. *Applied Mechanics Reviews, 49*, 155–199.

Noor, A. K., Burton, W., & Peters, J. M. (1991). Assessment of computational models for multilayered composite cylinders. *International Journal of Solids and Structures, 27*, 1269–1286.

Pagano, N. (1970). Exact solutions for rectangular bidirectional composites and sandwich plates. *Journal of Composite Materials, 4*, 20–34.

Palazotto, A. N., & Dennis, S. T. (1992). *Nonlinear analysis of shell structures*. Washington, DC: AIAA Series.

Pandya, B., & Kant, T. (1988). Flexural analysis of laminated composites using refined higher-order plate bending elements. *Computer Methods in Applied Mechanics and Engineering, 66*, 173–198.

Ramtekkar, G. S., Desai, Y. M., & Shah, A. H. (2002). Mixed finite-element model for thick composite laminated plates. *Mechanics of Advanced Materials and Structures, 9*, 133–156.

Ramtekkar, G. S., Desai, Y. M., & Shah, A. H. (2003). Application of a three-dimensional mixed finite element model to the flexure of sandwich plate. *Computers and Structures, 81*, 2183–2198.

Reddy, J. N. (1984). A simple higher-order theory for laminated composite plates. *Journal of Applied Mechanics, 51*, 745–752.

Reddy, J. N. (1989). On refined computational models of composite laminates. *International Journal for Numerical Methods in Engineering, 27*, 361–382.

Roy, A. K., & Sihn, S. (2001). Development of a three-dimensional mixed variational model for woven composites. I. Mathematical formulation. *International Journal of Solids and Structures, 38*, 5935–5947.

Sedira, L., Ayad, R., Sabhi, H., Hecini, M., & Sakami, S. (2012). An enhanced discrete Mindlin finite element model using a zigzag function. *European Journal of Computational Mechanics, 21*, 122–140.

Sihn, S., & Roy, A. K. (2001). Development of a three-dimensional mixed variational model for woven composites. II. Numerical solution and validation. *International Journal of Solids and Structures, 38*, 5949–5962.

Simo, J., Rifai, M., & Fox, D. (1990). On a stress resultant geometrically exact shell model. Part IV: Variable thickness shells with through-the-thickness stretching. *Computer Methods in Applied Mechanics and Engineering, 81*, 91–126.

Sze, K. Y., & Ghali, A. (1993). A hybrid brick element with rotational degrees of freedom. *Computational Mechanics, 12*, 147–163.

Van Hoa, S., & Feng, W. (1998). *Hybrid finite element method for stress analysis of laminated composites*. New York, NY: Springer Science, Kluwer Academic Publishers.

Whitney, J., & Pagano, N. (1970). Shear deformation in heterogeneous anisotropic plates. *Journal of Applied Mechanics, 37*, 1031–1036.

Yang, H. T. Y., Saigal, S., Masud, A., & Kapania, R. K. (2000). A survey of recent shell finite elements. *International Journal for Numerical Methods in Engineering, 47*, 101–127.

Yunus, S. M., Pawlak, T. P., & Cook, R. D. (1991). Solid elements with rotational degrees of freedom: Part I – Hexahedron elements. *International Journal for Numerical Methods in Engineering, 31*, 573–592.

Zhang, Y., & Yang, C. (2009). Recent developments in finite element analysis for laminated composite plates. *Composite and Structures, 88*, 147–157.